IEEE Photonics Journal
An IEEE Photonics Society Publication

Open Access

Intensity Demodulation Based Fiber Sensor for Dynamic Measurement of Acoustic Wave and Lateral Pressure Simultaneously

Volume 8, Number 6, December 2016

Xin Fu
Ping Lu
Wenjun Ni
Li Liu
Hao Liao
Deming Liu
Jiangshan Zhang

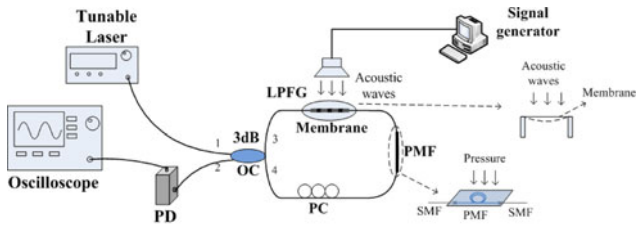

Experimental setup of the proposed sensor

DOI: 10.1109/JPHOT.2016.2627546
1943-0655

Intensity Demodulation Based Fiber Sensor for Dynamic Measurement of Acoustic Wave and Lateral Pressure Simultaneously

Xin Fu,[1,2] Ping Lu,[1,2] Wenjun Ni,[1,2] Li Liu,[1,2] Hao Liao,[1,2] Deming Liu,[1,2] and Jiangshan Zhang[3]

[1]Wuhan National Laboratory for Optoelectronics, Huazhong University of Science and Technology, Wuhan 430074, China
[2]School of Optical and Electronic Information, National Engineering Laboratory for Next Generation Internet Access System, Huazhong University of Science and Technology, Wuhan 430074, China
[3]Department of Electronics and Information Engineering, Huazhong University of Science and Technology, Wuhan 430074, China

DOI:10.1109/JPHOT.2016.2627546

Manuscript received October 29, 2016; accepted November 7, 2016. Date of publication November 10, 2016; date of current version November 28, 2016. This work was supported in part by the National Natural Science Foundation of China under Grant 61290315 and Grant 61275083 and in part by the Fundamental Research Funds for the Central Universities (HUST: No. 2014CG002). Corresponding author: P. Lu (e-mail: pluriver@mail.hust.edu.cn).

Abstract: In this paper, we propose an intensity demodulation based fiber sensor for dual-parameters sensing of acoustic wave and lateral pressure. The sensor consists of a long period fiber grating (LPFG) inserted into a Sagnac interferometer (SI). The LPFG is kept straight and fixed on a polyethylene terephthalate membrane for acoustic detection. A tunable laser source (TLS) is utilized to illuminate the sensor. The acoustic wave will produce a time-varying intensity signal that consists of an alternating current (ac) component and a direct current (dc) component. The ac component contains the acoustic information, while the dc level is determined by the transmittance of the sensor in the static condition (without acoustic signal applied on the sensor). Since the lateral pressure induced wavelength shift of the SI will change the transmittance at the TLS wavelength, the dc level varies with different lateral pressure applied on the sensor. Therefore, the acoustic wave and lateral pressure can be demodulated, respectively, by monitoring the ac component and dc level in the output signal. In the experiment, output time-domain signals with 500 Hz ac components and different dc values are acquired when 500 Hz acoustic wave and different lateral pressure is applied on the sensor.

Index Terms: Long period fiber grating (LPFG), Sagnac interferometer (SI), dual-parameters sensing, acoustic wave, lateral pressure.

1. Introduction

Pressure and acoustic waves are very important parameters in many applications. Effective measurement of pressure is of great significance in the fields such as structure health monitoring, disaster forecast, oil pipeline leakage detection, etc. For example, abnormal pressure variations in the underground will arise before an earthquake [1]. Among numerous sensing methods, fiber

sensing technology has shown many attracting advantages such as small size, light weight, immunity to electromagnetic interference, and the ability of distributed sensing and multiplexing. Due to these mentioned advantages over electric and mechanical techniques, the fiber pressure sensor has been widely studied. Fabry-Perot interferometer (FPI) based fiber pressure sensor is simple but effective [2]–[6]. Researchers have also proposed effective methods for pressure sensing based on different techniques such as fiber Bragg grating (FBG) [7], CO2-laser induced long-period fiber grating [8] and intensity modulation [9]. Of equal importance to pressure sensing, acoustic detection has also attracted a lot of attention. Acoustic signals will also be produced in different kinds of disasters [10], [11]. Diaphragm based FPI acoustic sensor is a common method studied by researchers [12]–[15]. Other types of fiber devices such as non-fused fiber coupler [16], fiber laser [17], [18], phase-shifted fiber Bragg grating [19], and micro fiber knot [20] have also been demonstrated for acoustic sensing.

Another hotspot in the research of fiber sensing is dual-parameters measurement. The conventional mechanism of simultaneous measurement of two parameters is based on two reference wavelengths. Usually the two reference wavelengths are resonant dips or peaks caused by different effects such as mode interference or wavelength dependent loss, etc. Due to different effects, the two reference wavelengths have different sensitivities to each parameter. By introducing a matrix, the two measurands can be calculated from the different responses of the two wavelengths. Researchers have proposed different ways to realize simultaneous measurement of different parameters such as temperature and strain [21], [22], temperature and refractive index (RI) [23]–[25], temperature and curvature [26], temperature and displacement [27], strain and lateral stress [28], etc. However, as mentioned above, since the conventional dual-parameters sensing is based on wavelength demodulation, it can hardly implement simultaneous measurement for dynamic parameters such as acoustic wave and vibration.

In this paper, we investigated a more generalized method for simultaneous measurement of dynamic acoustic signal and static lateral pressure based on intensity demodulation. The output intensity of the sensor is modulated by the acoustic wave. Since the acoustic signal is dynamic, it produces the AC component. The AC component contains the information of the acoustic wave. Lateral pressure applied on the sensor will lead to a wavelength shift of the interference spectrum of the SI. The wavelength shift is converted to an intensity variation by a TLS. The lateral pressure variation is usually very slow compared to the acoustic frequency, so it can be regarded as a static parameter. Therefore, the pressure induced intensity variation is embodied in the DC level change of the output signal. The mechanism is analyzed in detail. The experiment is conducted and the results can verify the feasibility of our proposed method. The time-domain responses to 500 Hz acoustic signals with different lateral pressure applied on the sensor is tested. The minimum detectable acoustic pressure is 331.9 μPa/Hz$^{1/2}$. DC value of the output signal is in a linear relationship with the lateral pressure and the sensitivity is 40 mV/kPa. Compared to the traditional wavelength tracking technique, our proposed sensor exhibits the capability for dual-parameters sensing for dynamic parameters such as sound or vibration.

2. Basic Structure and Sensing Mechanism

In our proposed sensor structure, the LPFG is inserted into a polarization-maintaining photonic crystal fiber (PM-PCF) based Sagnac interferometer (SI), as shown in Fig. 1. Light injected into the PMF will propagate along two orthogonal polarization states owing to the high birefringent coefficient. A phase difference between the two polarization states is accumulated during the propagation in the PMF owing to the refractive index (RI) difference of two polarization states. When the two counter-propagating beams in the SI meet each other again at the coupler after a round-trip propagation, interference will occur.

For acoustic detection, a PET membrane is adopted as a transducer. The LPFG is fixed on the membrane. The acoustic wave will generate the vibration of the membrane. The LPFG fixed on the membrane will vibrate in accompany with it. The vibration of the LPFG is equivalent to a dynamic curvature modulation, as shown in Fig. 2(a). When the LPFG is bent, the intensity of the

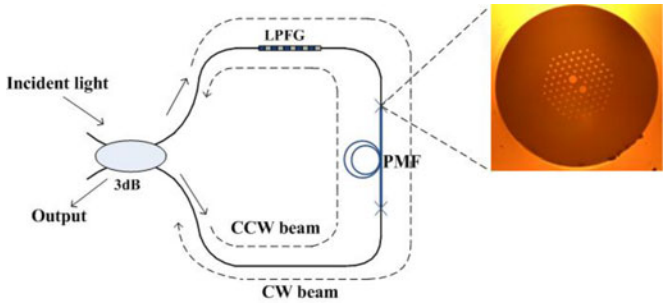

Fig. 1. Basic structure of the proposed sensor.

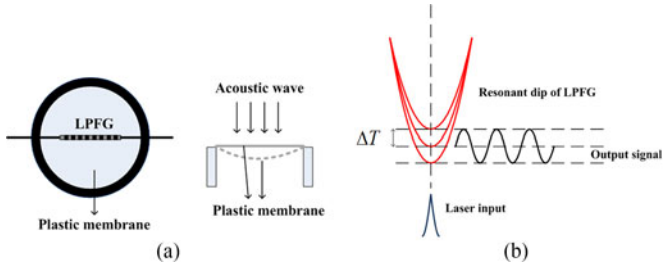

Fig. 2. (a) Structure and principle of the membrane transducer. (b) Principle of intensity modulation.

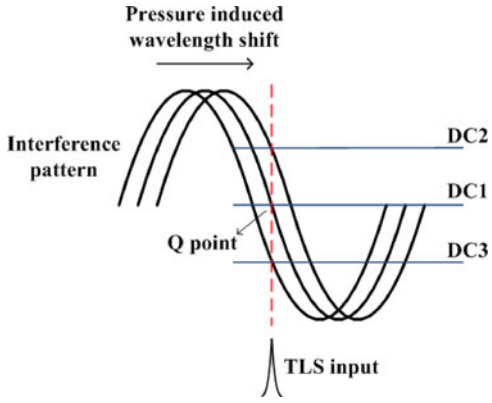

Fig. 3. Relationship between the intensity level and wavelength shift induced by the lateral pressure.

resonant dip varies while the resonant wavelength remains almost unchanged [29]. By employing a TLS and tune the wavelength to the resonant dip of the LPFG, the output signal will be a time-varying waveform when the LPFG is utilized for the acoustic measurement, thus producing the AC component. The principle is exhibited in Fig. 2(b).

If lateral pressure is applied on the SI, the RI difference between the two orthogonal polarization states in the PMF is changed because of the elasto-optical effect. This will lead to a wavelength shift of the interference pattern [28]. The single wavelength TLS can transfer the wavelength shift to an intensity variation. Since the variation of the pressure is much slower compared to the acoustic frequency, the pressure induced intensity variation causes the DC level change. If the TLS wavelength locates at the middle of the linear region (Q point) of the interference pattern, the relationship between the DC level and the pressure induced wavelength shift will be approximately linear in a specific range, as shown in Fig. 3.

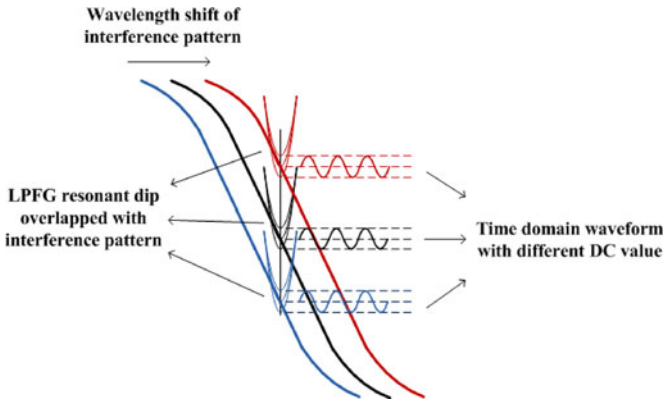

Fig. 4. Schematic diagram of the mechanism for dynamic dual-parameters sensing.

The output intensity signal is composed of two parts, namely, the AC component and the DC component. Since the PMF is not put on the transducer membrane, it will not respond to the acoustic vibration. So the AC component is produced only by the dynamic vibration of the LPFG caused from the acoustic signal, while the DC component is the output intensity level when the sensor is not exposed to acoustic waves.

According to the analysis above, if the resonant wavelength of the LPFG is at the Q point of the SI interference spectrum and the TLS is tuned to that wavelength, the dynamic acoustic signal and static lateral pressure can be measured simultaneously by monitoring the output intensity signal. The information of acoustic signals consist in the AC component, while the DC level reflects the lateral pressure applied on the sensor. Therefore, the two parameters can easily be measured at the same time. The schematic diagram is shown in Fig. 4 below and it clearly reveals how the dynamic acoustic signal and static lateral pressure can be demodulate from the DC and AC components.

The detailed analysis of the mechanism are as follows.

Since the LPFG is inserted into the Sagnac loop interferometer, the transmission function of the proposed sensor structure should be the multiplication of the transmission function of LPFG and SI. The transmission functions of the LPFG and the SI are respectively expressed in the following equations:

$$T_{LPFG} = \cos^2(l \cdot \sqrt{\eta^2 + \delta^2}) + \frac{\delta^2}{\eta^2 + \delta^2} \sin^2(l \cdot \sqrt{\eta^2 + \delta^2}) \tag{1}$$

$$T_{SI} = \sin^2(\theta_1 + \theta_2) \cos^2 \frac{\pi \Delta n L}{\lambda}. \tag{2}$$

Therefore, the transmission function of the proposed sensor can be written as

$$T = T_{LPFG} \cdot T_{SI}. \tag{3}$$

In the equation, l and L is the length of the LPFG and the PMF, respectively. θ_1 and θ_2 is the angle of polarization states rotated at the joints of the PMF and SMF. η and δ represents the AC and DC coupling coefficient of the LPFG. $\triangle n$ is the effective RI difference of the two orthogonal polarization axes in the PMF.

According to the theory of long period fiber grating, the DC coupling coefficient is zero at the resonant wavelength of the LPFG, i.e. $\delta = 0$. Therefore, the transmittance of the LPFG is as follows:

$$T_{LPFG} = \cos^2(\eta l). \tag{4}$$

Assume that the resonant wavelength of the LPFG is located at the Q point of the interference pattern of SI, which means $\cos^2(\pi \triangle n_0 L / \lambda) = 1/2$, and therefore, we can suppose the phase difference to be $\pi \triangle n_0 L / \lambda = k\pi + \pi/4$. $\triangle n_0$ is the initial effective RI difference. In order to make

the analysis simple, we can assume $\sin^2(\theta_1 + \theta_2)$ to be 1, and this factor can be adjusted by the polarization controller (PC). So the initial transmission function of the sensor should be expressed as

$$T_0 = \frac{1}{2}\cos^2(\eta l). \tag{5}$$

When the LPFG responds to the acoustic signal, the intensity of the resonant dip will vary with the acoustic frequency in the time domain due to the dynamic curvature modulation, as demonstrated in Fig. 2. This can be expressed as follows:

$$T_{LPFG}{}' = T_{LPFG} + \Delta T \cdot \cos(\omega t). \tag{6}$$

In (6), $\triangle T$ is the acoustic induced transmittance variation of the LPFG. When lateral pressure is applied on the proposed sensor, the induced phase difference and the transmission function is derived as follows:

$$\varphi' = \frac{\pi(\Delta n_0 + \Delta n_p)L}{\lambda} = k\pi + \frac{\pi}{4} + \frac{\pi \Delta n_p L}{\lambda} \tag{7}$$

$$T_{SI}{}' = \cos^2\varphi' = \frac{1}{2} + \frac{1}{2}\sin\left(\frac{\pi \Delta n_p L}{\lambda}\right). \tag{8}$$

In (7) and (8), $\triangle n_p$ is the pressure induced variation of the effective RI difference between the two axes of the PMF. In the linear region of the interference fringes, the function can be operated approximately:

$$T_{SI}{}' \approx \frac{1}{2} + \frac{1}{2} \cdot \frac{\pi \Delta n_p L}{\lambda}. \tag{9}$$

Therefore, under the simultaneous impact of the acoustic waves and lateral pressure, the transmission function can be written as

$$\begin{aligned} T &= \left(\frac{1}{2} + \frac{1}{2} \cdot \frac{\pi \Delta n_p L}{\lambda}\right) \cdot [\cos^2(\eta l) + \Delta T \cdot \cos(\omega t)] \\ &= T_{DC} + T_{AC} \end{aligned} \tag{10}$$

$$T_{DC} = \left(\frac{1}{2} + \frac{1}{2} \cdot \frac{\pi \Delta n_p L}{\lambda}\right) \cdot \cos^2(\eta l),$$

$$T_{AC} = \left(\frac{1}{2} + \frac{1}{2} \cdot \frac{\pi \Delta n_p L}{\lambda}\right) \cdot \Delta T \cdot \cos(\omega t). \tag{11}$$

For a certain LPFG, $\cos^2(\eta l)$ is a constant. It can be seen that the transmittance of the proposed sensor is composed of DC component T_{DC} and AC component T_{AC}. The DC component only varies with the lateral pressure, while the AC component depends on both the lateral pressure and acoustic signals. The frequency of the AC part is equal to the acoustic frequency, but the AC amplitude is relevant to both acoustic signals and lateral pressure. Suppose the lateral pressure induced RI change and acoustic induced transmission variation to be

$$\Delta n_p = \sigma \cdot P, \ \Delta T = k \cdot p \tag{12}$$

where σ and k are two constant coefficients. The lateral pressure and acoustic signal can be derived and expressed by the DC and AC components as follows:

$$P = \frac{2\lambda(T_{DC} - T_0)}{\pi\sigma L \cos^2(\eta l)} \tag{13}$$

$$p\cos(\omega t) = T_{AC}/k \cdot \left[\frac{1}{2} + \frac{T_{DC} - T_0}{\cos^2(\eta l)}\right]. \tag{14}$$

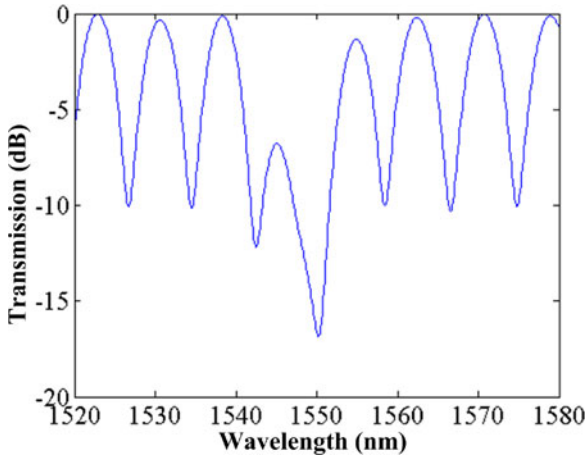

Fig. 5. Simulated spectrum of the proposed sensor.

From (13) and (14), the DC level has a linear relationship with the lateral pressure. The frequency of the AC component is equal to the acoustic frequency, while the AC amplitude is relevant to both lateral pressure and amplitude of acoustic signal.

In the simulation, by adjusting the resonant wavelength of LPFG to be 1548 nm, which is at the middle of the hypotenuse of the interference pattern, the simulated transmission spectrum can be calculated and demonstrated in the Fig. 5.

In order to demonstrate the schematic of evolution under acoustic and lateral pressure, other two simulations have been conducted. Firstly, we simulated the spectral response with different $\triangle n_p$ caused by different lateral pressure. The simulation result is shown in Fig. 6(a). The three curves of different color (blue, red and black) represent the sensor's optical spectrum under different lateral pressure. An obvious wavelength shift can be observed in the simulated transmission spectrum, agree with the analysis we have discussed above. On the operating point of 1548 nm (resonant wavelength of LPFG and Q point of the SI spectrum in the simulation), an intensity variation comes into being due to the wavelength shift, as demonstrated by DC1, DC2, and DC3 in Fig. 6(a). Afterward, we simulated the spectral response under the impact of lateral pressure and acoustic wave. Since the optical spectrum shows the static condition of the sensor, while acoustic is a dynamic parameter, and therefore, it is difficult to demonstrate the sensor's response to acoustic on the simulated spectrum. According to the analysis in the preceding part of this text, the LPFG's response to acoustic wave is based on the curvature modulation that will change the intensity of the resonant dip. Therefore, alternatively, we conducted a simulation on the spectrum under different lateral pressure and different intensity of LPFG's resonant dip. The simulated result is exhibited in Fig. 6(b). Similar to Fig. 6(a), the curves of different color (blue, red and black) are the spectrums under different lateral pressure. The three curves of each color indicate the response of the spectrum with different LPFG's intensity under the same lateral pressure. As plotted in the Fig. 6(b), it is clear that the lateral pressure induced wavelength shift of the interference spectrum leads to different DC levels, while the acoustic signal is demodulated by the AC component. The simulation results can identify the feasibility of our proposed sensor.

3. Experimental Setup and Operation Principle

The experimental setup is demonstrated in Fig. 7. The incident light from the TLS is split into two counter-propagating beams by the 3 dB fiber coupler. A section of PMF is fusion spliced between port3 and port4 of the coupler to form a normal SI. The LPFG is inserted into the SI. A PC is employed to adjust the polarization states in the SI in order to achieve a good contrast of the interference

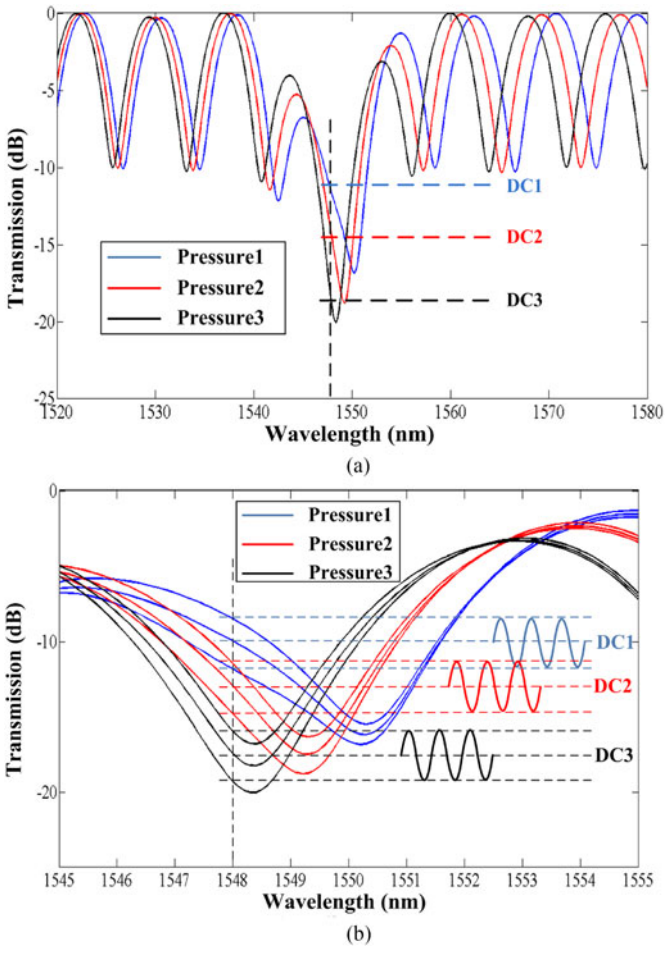

Fig. 6. (a) Simulated spectrum response under different lateral pressure. (b) Simulated spectrum response under different lateral pressure and different intensity of LPFG's resonant dip.

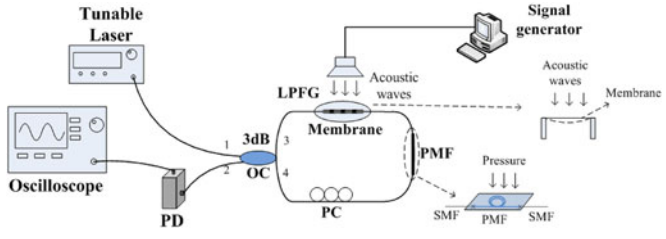

Fig. 7. Experimental setup of the proposed sensor.

pattern. A signal generator drives the loudspeaker to produce sinusoidal acoustic signals of single frequency. As discussed in the previous part2, the LPFG is fixed upon a PET membrane and kept straight. The LPFG we used in our experiment has a grating period of 625 μm, and the resonant wavelength is 1548.6 nm. It is fabricated by UV light inscription on a hydrogen-loaded fiber via a phase mask. These factors of the LPFG may affect the resonant wavelength. But as analyzed in part2, the simultaneous measurement can be achieved as long as the resonant wavelength of the LPFG locates at the Q point of the interference spectrum of the SI. Therefore, by controlling the SI, the experimental results will not be affected even if another LPFG with different parameters is used.

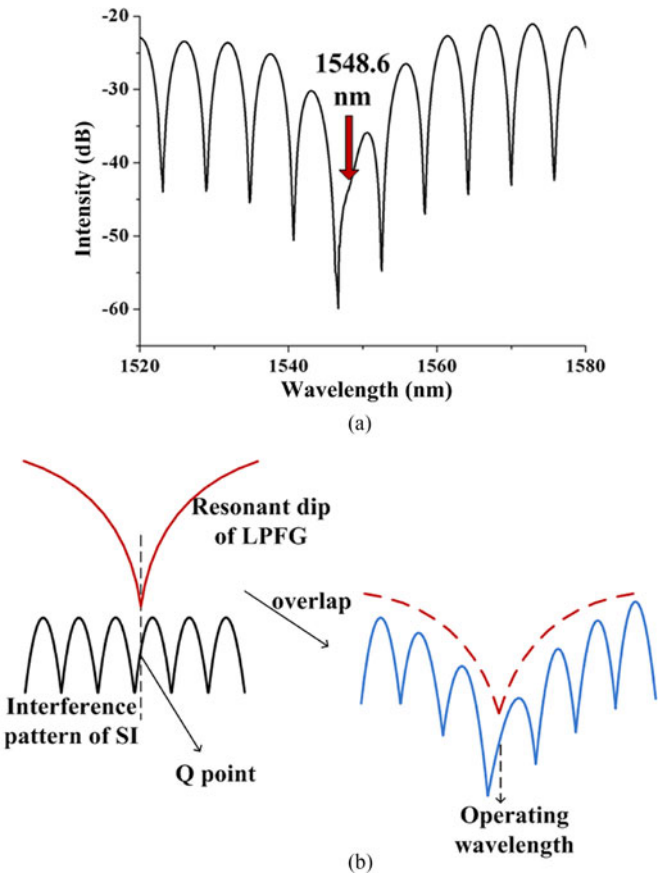

Fig. 8. (a) Transmission spectrum of the sensor. (b) Spectrum overlap.

Based on the above analysis, the resonant wavelength of the LPFG should be adjusted to the Q point of the SI interference pattern. Therefore, first, firstly we adopt a broadband source (BBS) to illuminate the sensor and observe the spectrum on the optical spectrum analyzer (OSA, Yokogawa AQ6370c). When the spectrum of the sensor is proper for our experiment, a TLS is then used to replace the BBS to illuminate the sensor. The output intensity is detected by a photodetector (PD). The PD converts the intensity of the optical signal to electric signal and displayed on an oscilloscope. In the experiment, we test the response of the sensor to acoustic signals in a frequency range, as well as acoustic signals with different lateral pressure applied.

4. Experiment Results and Discussion

The experimental setup is shown in Fig. 7. The resonant wavelength of the LPFG in our structure is 1548.6 nm. Fig. 8(a) reveals the transmission spectrum recorded by the OSA, in which we can see that the wavelength of 1548.6 nm is on the Q point of the interference spectrum, similar to the simulated results in Fig. 5. In the spectrum, the resonant dip of the LPFG can't be seen on 1548.6 nm. This is due to the overlap of the resonant dip with the SI interference pattern, and the wavelength of the dip is on the hypotenuse of the interference spectrum, as illustrated in Fig. 8(b).

The experiment of simultaneous measurement of acoustic and lateral pressure is then conducted. Sinusoidal acoustic signals of 500 Hz is applied on the sensor along with different lateral pressure. The time-domain intensity signals are detected by the PD and shown in Fig. 9(a). The AC components of the detected intensity signals all have a same frequency of 500 Hz, which is the

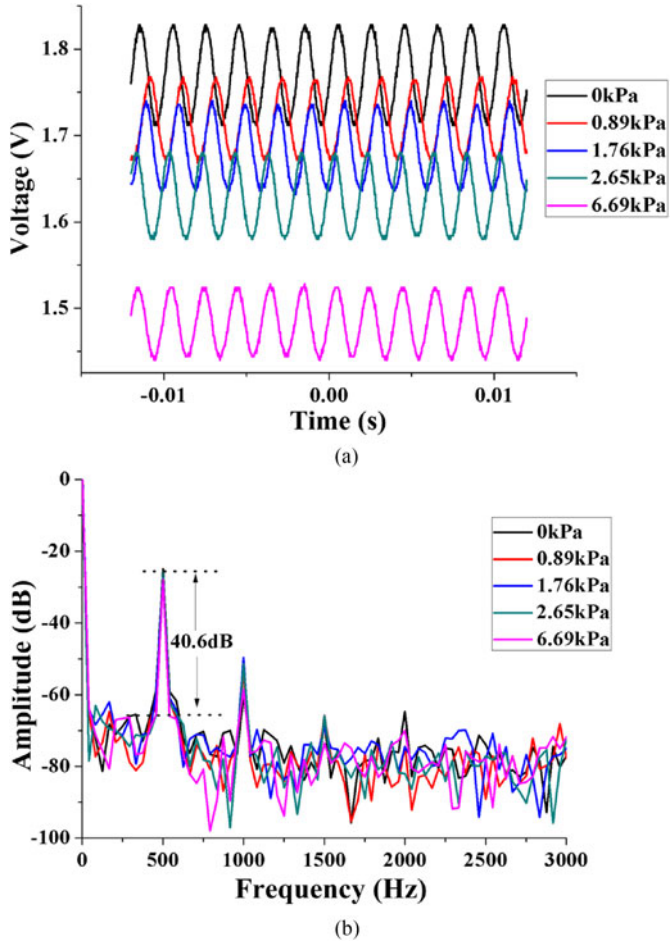

Fig. 9. (a) Time domain waveform of 500 Hz under different pressure. (b) Fourier spectrum under different pressure.

same as the acoustic frequency. The DC levels are varying with different lateral pressure applied on the sensing structure. The frequency spectrums are acquired by taking the FFT of the time-domain signals and shown in Fig. 9(b). The Fourier spectrums of the acquired time-domain signals under different lateral pressure are almost the same and all show a main peak at 500 Hz with the consistent signal to noise ratio (SNR) of 40.6 dB, indicating that the pressure has scarcely cross interference on the acoustic detection. The acoustic pressure is 75 dB, which is measured by a sound level meter. The 3 dB bandwidth of the Fourier spectrum is 10 Hz, and therefore, it can be calculated that the minimum detectable acoustic pressure is 331.9 μPa/Hz$^{1/2}$.

The DC levels and AC amplitudes of the detected signal under different pressure is plotted in Fig. 10. The linear fit shows that the pressure sensitivity of DC values and AC amplitudes are 40 mV/kPa and 4 mV/kPa, respectively. As analyzed in the part3, the DC level has a linear relationship with the lateral pressure, while the AC amplitude is relevant to both acoustic signal amplitude and lateral pressure. The experimental results show that the pressure sensitivity of AC amplitudes to the lateral pressure are one order of magnitude lower than that of DC value, and therefore, the cross interference of the pressure to the AC amplitudes are very small and can be neglected.

As mentioned above, the PMF is not fixed on the PET membrane; therefore, it will not introduce a cross-effect with the LPFG on acoustic sensing. In order to study the cross-sensitivity between the LPFG and PMF on the lateral pressure sensing, we then carry out an experiment to apply the

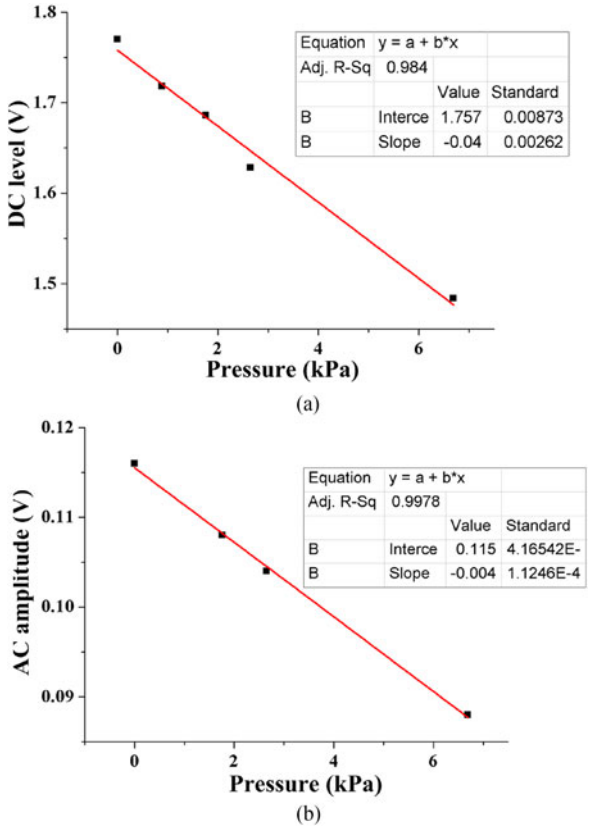

Fig. 10. Relationship between pressure and (a) DC value. (b) AC amplitude.

lateral pressure on the LPFG and PMF individually. The response of the transmission spectrum is recorded by using a BBS and OSA. Fig. 11(a) and (b), respectively, demonstrates the spectrum response when the lateral pressure is applied on the PMF and LPFG. An obvious wavelength shift can be observed when the PMF is under different pressure, leading to an intensity variation at the wavelength of 1548.6 nm, which is the operating wavelength when measuring acoustic wave and lateral pressure simultaneously. When different pressure is applied on the LPFG, the whole spectrum stays almost unchanged. Only very little wavelength shift of the interference spectrum can be observed. From the previous theoretical analysis, the interference pattern is only caused by the birefringence of the PMF in the SI, while the LPFG is irrelevant with the interference. Therefore, the possible reason for the very little wavelength shift is that the lateral pressure induces a very small birefringence in the LPFG. The intensity variation at the wavelength of 1548.6 nm is shown in Fig. 12.

It can be seen from Fig. 12 that the pressure sensitivity is 1.8 dB/kPa and 0.27 dB/kPa for the PMF and LPFG, respectively. The sensitivity of the PMF to the pressure is more than six times larger than that of the LPFG, so the cross-sensitivity is relatively small. In practical applications, proper design of the packaging may be possible to insulate the LPFG from the pressure variation so that the cross-sensitivity is able to be further reduced.

As for the influence of the temperature, the PM-PCF is insensitive to the temperature variation because of the air-hole structure, and therefore, we tested the temperature response of the LPFG. In the range of 20-55° C, the wavelength shift of the LPFG's resonant dip is 2.2 nm with a sensitivity of 0.067 nm °C. Therefore, In the normal range of the environmental temperature, the wavelength shift of the LPFG is about 1-2 nanometers, so the resonant dip will still locate in the linear region of the

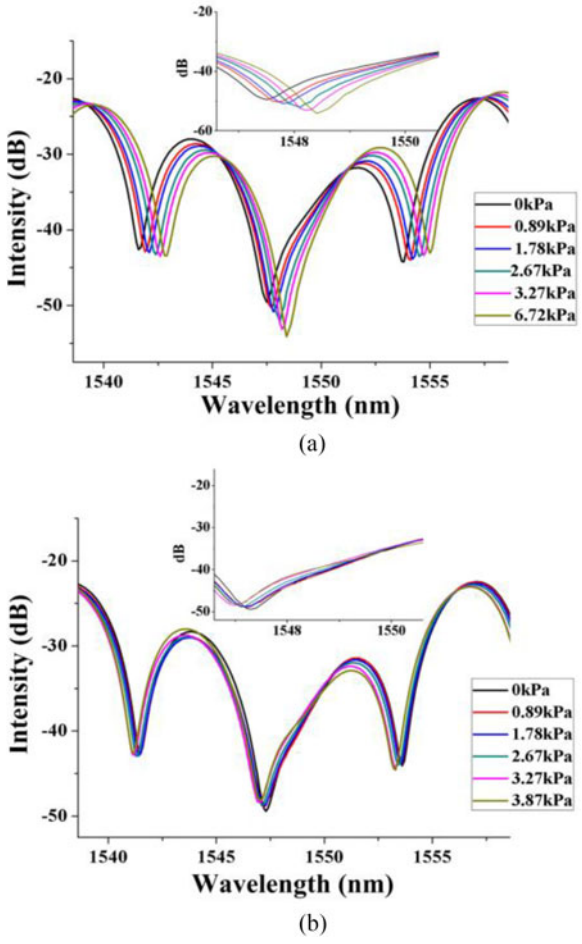

Fig. 11. Spectrum response when the lateral pressure is added on (a) PMF. (b) LPFG.

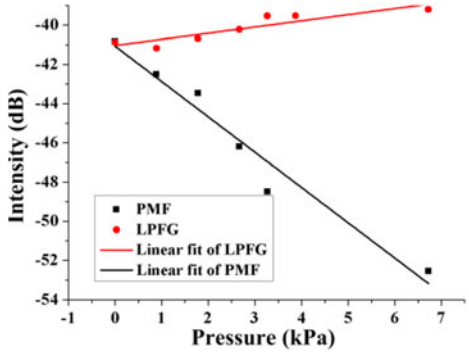

Fig. 12. Intensity variation at the wavelength of 1548.6 nm with lateral pressure.

interference spectrum. If the sensor works in a harsh environment that suffers a larger temperature range, extra technique for temperature compensation will be needed.

Another noteworthy point is that the polarization-maintaining fiber based pressure sensor would suffer an orientation-dependent sensitivity. In this paper, the PMF is coiled for the lateral pressure measurement, so that the PMF can be sufficiently affected by the pressure. The orientation of the lateral pressure measured by the PMF should be vertical to the coil plane. For a certain PMF coil,

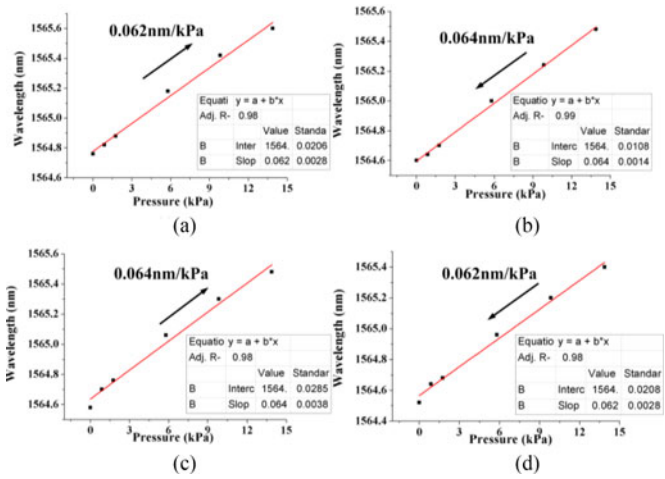

Fig. 13. Lateral pressure sensitivity when the pressure is repeatedly increasing and decreasing.

the pressure orientation is stationary relative to the PMF, and therefore, the sensitivity should be a constant in theory. In order to prove the stability of the pressure sensitivity, we conducted an experiment by increasing and decreasing the lateral pressure on the PMF coil repeatedly. The time interval between each time of pressure increasing and decreasing is half an hour. The spectrum is monitored by the OSA and demonstrated in Fig. 13. The sensitivity of the four times increasing and decreasing lateral pressure is 0.062 nm/kPa, 0.064 nm/kPa, 0.064 nm/kPa, 0.062 nm/kPa, respectively.

5. Conclusion

To summarize, we proposed a novel fiber sensor for dual-parameters sensing of acoustic wave and lateral pressure. Different from the traditional method of simultaneous measurement of two static parameters by wavelength demodulation technique, we applied the simple intensity demodulation method to detect the time-varying parameter. The acquired intensity signal from the PD is composed of DC and AC components for the detection of dynamic acoustic wave and static lateral pressure, respectively. The frequency and amplitude of the AC component contains the information of acoustic signal. The DC level reflects the static lateral pressure applied on the sensor. This method for dual-parameters sensing has the advantages such as simple demodulation scheme and capability of detecting dynamic signals. The proposed sensor for simultaneous measurement of acoustic and pressure has great potential in many applications such as hydroacoustics and earthquake detection, etc.

References

[1] R. H. Sibson, “Interactions between temperature and pore-fluid pressure during earthquake faulting and a mechanism for partial or total stress relief,” *Nature*, vol. 243, no. 126, pp. 66–68, 1973.
[2] K. Bremer, E. Lewis, G. Leen, B. Moss, S. Lochmann, and I. A. R. Mueller, “Feedback stabilized interrogation technique for EFPI/FBG hybrid fiber-optic pressure and temperature sensors,” *IEEE Sens. J.*, vol. 12, no. 1, pp. 133–138, Jan. 2012.
[3] H. Bae and M. Yu, “Miniature Fabry–Perot pressure sensor created by using UV-molding process with an optical fiber based mold,” *Opt. Exp.*, vol. 20, no. 13, pp. 14573–14583, 2012.
[4] M. Hou, Y. Wang, S. Liu, J. Guo, Z. Li, and P. Lu, “Sensitivity-enhanced pressure sensor with hollow-core photonic crystal fiber,” *J. Lightw. Technol.*, vol. 32, no. 23, pp. 4035–4039, Dec. 2014.
[5] J. Tang *et al.*, “High-sensitivity gas pressure sensor based on Fabry-Perot interferometer with a side opened channel in hollow-core photonic bandgap fiber,” *IEEE Photon. J.*, vol. 7, no. 6, Dec. 2015, Art. no. 6803307.

[6] C. Liao *et al.*, "Sub-micron silica diaphragm based fiber-tip Fabry-Perot interferometer for pressure measurement," *Opt. Lett.*, vol. 39, no. 10, pp. 2827–2830, 2014.
[7] V. r. Pachava, S. Kamineni, P. Kishore, and S. S. Madhuvarasu, "Enhanced sensitivity of FBG pressure sensor using thin metal diaphragm," in *Proc. Int. Conf. Fibre Opt. Photon.*, 2012, Art. no. TPo.20.
[8] J. Tang *et al.*, "Gas pressure sensor based on CO2-laser-induced long-period fiber grating in air-core photonic bandgap fiber," *IEEE Photon. J.*, vol. 7, no. 5, Oct. 2015, Art. no. 6803107.
[9] P. Nath, S. K. Neog, R. Biswas, and A. Choudhury, "All fiber-optic sensor for monitoring pressure fluctuations in ON/OFF state," *IEEE Sens. J.*, vol. 13, no. 4, pp. 1148–1152, Apr. 2013.
[10] T. Mikumo, M. Garces, T. Shibutani, W. Morii, T. Okawa, and Y. Ishihara, "Acoustic-gravity waves from the source region of the 2011 great Tohoku earthquake (Mw = 9.0)," *J. Geophys. Res.*, vol. 118, no. 4, pp. 1534–1545, 2013.
[11] H. Fujimoto, M. Kido, T. Iinuma, Y. Osada, and J. Yamamoto, "Extended GPS/Acoustic geodetic observation near the Japan trench axis for the study of the giant 2011 Tohoku-oki earthquake," in *Proc. IEEE Int. IEEE Underwater Tech. Symp.*, 2013, pp. 1–4.
[12] J. Ma, H. Xuan, HL. Ho, W. Jin, Y. Yang, and S. Fan, "Fiber-optic Fabry–Perot acoustic sensor with multilayer graphene diaphragm," *IEEE Photon. Technol. Lett.*, vol. 10, no. 25, pp. 932–935, May 2013.
[13] J. Ma, Y. Yu, and W. Jin, "Demodulation of diaphragm based acoustic sensor using Sagnac interferometer with stable phase bias," *Opt. Exp.*, vol. 23, no. 22, pp. 29268–29278, 2015.
[14] F. Xu, J. Shi, K. Gong, H. Li, R. Hui, and B. Yu, "Fiber-optic acoustic pressure sensor based on large-area nanolayer silver diaghragm," *Opt. Lett.*, vol. 39, no. 10, pp. 2838–2840, 2014.
[15] L. Liu *et al.*, "UV adhesive diaphragm-based FPI sensor for very low frequency acoustic sensing," *IEEE Photon. J.*, vol. 8, no. 1, Feb. 2016, Art. no. 6800709.
[16] S. Wang, P. Lu, L. Zhang, D. Liu, and J. Zhang, "Optical fiber acoustic sensor based on nonstandard fused coupler and aluminum foil," *IEEE Sens. J.*, vol. 14, no. 7, pp. 2293–2298, Jul. 2014.
[17] C. Lyu, C. Wu, HY. Tam, C. Lu, and J. Ma, "Polarimetric heterodyning fiber laser sensor for directional acoustic signal measurement," *Opt. Exp.*, vol. 21, no. 15, pp. 18273–18280, 2013.
[18] M. Han, T. Liu, L. Hu, and Q. Zhang, "Intensity-demodulated fiber-ring laser sensor system for acoustic emission detection," *Opt. Exp.*, vol. 21, no. 24, pp. 29269–29276, 2013.
[19] W. Qi and Y. Okabe, "High-sensitivity ultrasonic phase-shifted fiber Bragg grating balanced sensing system," *Opt. Exp.*, vol. 20, no. 27, pp. 28353–28362, 2012.
[20] J. M. De Freitas, T. A. Birks, and M. Rollings, "Optical micro-knot resonator hydrophone," *Opt. Exp.*, vol. 23, no. 5, pp. 5850–5860, 2015.
[21] R. A. Pérez-Herrera *et al.*, "Simultaneous measurement of strain and temperature based on clover microstructured fiber loop mirror," *Measurement*, vol. 65, pp. 50–53, 2015.
[22] B. Dong, Y. Peng, Y. Wang, and C. Yu, "Mode division multiplexing in a fiber modal interferometer for dual-parameters measurement," *IEEE Photon. Technol. Lett.*, vol. 28, no. 2, pp. 143–146, Jan. 2016.
[23] P. Lu, J. Harris, Y. Xu, Y. Lu, L. Chen, and X. Bao, "Simultaneous refractive index and temperature measurements using a tapered bend-resistant fiber interferometer," *Opt. Lett.*, vol. 37, no. 22, pp. 4567–4569, 2012.
[24] Q. Sun, H. Luo, H. Luo, M. Lai, D. Liu, and L. Zhang, "Multimode microfiber interferometer for dual-parameters sensing assisted by Fresnel reflection," *Opt. Exp.*, vol. 23, no. 10, pp. 12777–12783, 2015.
[25] X. Yu, X. Chen, D. Bu, J. Zhang, and S. Liu, "In-fiber modal interferometer for simultaneous measurement of refractive index and temperature," *IEEE Photon. Technol. Lett.*, vol. 28, no. 2, pp. 189–192, Jan. 2016.
[26] Y. Zhou *et al.*, "Simultaneous measurement of curvature and temperature based on PCF-based interferometer and fiber Bragg grating," *Opt. Commun.*, vol. 284, no. 24, pp. 5669–5672, 2011.
[27] Q. Rong, X. Qiao, J. Zhang, R. Wang, M. Hu, and Z. Feng, "Simultaneous measurement for displacement and temperature using fiber Bragg grating cladding mode based on core diameter mismatch," *J. Lightw. Technol.*, vol. 30, no. 11, pp. 1645–1650, 2012.
[28] S. Wang, P. Lu, L. Mao, D. Liu, and S. Jiang, "Cascaded interferometers structure based on dual-pass Mach–Zehnder interferometer and Sagnac interferometer for dual-parameter sensing," *Opt. Exp*, vol. 23, no. 2, pp. 674–680, 2015.
[29] K. Tan, C. Chan, S. C. Tjin, and X. Dong, "Embedded long-period fiber grating bending sensor," *Sensor Actuat. A-Phys.*, vol. 125, no. 2, pp. 267–272, 2006.